22. Tauzher, G.; Amiconi, G.; Antonini, E.; Grunori, M.; Costa, G. *Nature New Biology* **1973**, *241*, 222.
23. Bayer, E. *Chem. Ber.* **1957**, *90*, 2325.
24. Bayer, E. *Angew. Chem. Internat. Edit.* **1964**, *3*, 325.
25. Earnshaw, A.; Hewlett, P. C.; Larkworthy, L. F. *J. Chem. Soc.* **1965**, 4718.
26. Bard, A. J.; Faulkner, L. R. *Electrochemical Methodes*; Wiley: New York, 1990, Chap. 6.
27. Gubbins, K.; Walker, R. *J. Electrochem. Soc.* **1964**, *112*, 469.
28. Costa, G.; Puxeddu, A.; Stefani, L. B. *Inorg. Nucl. Chem. Lett.* **1970**, *6*, 191.
29. Andrieux, C. P.; Saveant, J. M. *J. Electroanal. Chem.* **1982**, *142*, 1.
30. Koutecky, J.; Levich, V. G. *Zh. Fiz. Khim.* **1956**, *32*, 1565.
31. Ohsaka, T.; Watanabe, T.; Kitamura, F.; Oyama, N.; Tokuda, K. *J. Chem. Soc., Chem. Commun.* **1991**, 489.
32. Griffiths, J. S. *Proc. Roy. Soc.* **1956**, *(A) 235*, 23.
33. Pauling, L. *Nature* **1964**, *203*, 182.
34. Collman, J. P.; Denisovich, P.; Konai, Y.; Marrocco, M.; Koval, C.; Anson, F. *J. Am. Chem. Soc.* **1980**, *103*, 6027.

Molecular Dynamics Simulation Studies of Zeolite A. VI. Vibrational Motion of Non-Rigid Zeolite-A Framework

Song Hi Lee* and Sang Gu Choi†

Department of Chemistry, Kyungsung University, Pusan 608-736, Korea
†Department of Industrial Safety, Yangsan Junior College, Yangsan 626-040, Korea
Received October 29, 1997

In the present paper, we report a molecular dynamics (MD) simulation of non-rigid zeolite-A framework only as the base case for a consistent study of the role of intraframework interaction on several zeolite-A systems using the same technique in our previous studies of rigid zeolite-A frameworks. Usual bond stretching, bond angle bending, torsional rotational, and non-bonded Lennard-Jones and electrostatic interactions are considered as intraframework interaction potentials. The comparison of experimental and calculated structural parameters confirms the validity of our MD simulation for zeolite-A framework. The radial distribution functions of non-rigid zeolite-A framework atoms characterize the vibrational motion of the framework atoms. Mean square displacements are all periodic with a short period of 0.08 ps and a slow change in the amplitude of the vibration with a long period of 0.53 ps. The displacement auto-correlation (DAC) and neighbor-correlation (DNC) functions describe the up-and-down motion of the framework atoms from the center of α-cage and the back-and-forth motion on each ring window from the center of each window. The DAC and DNC functions of the framework atoms from the center of α-cage at the 8-ring windows have the same period of the up-and-down motion, but those functions from the center of 8-ring window at the 8-ring windows are of different periods of the back-and-forth motion.

Introduction

The development of accurate, widely applicable, predictive methods for physico-chemical properties estimation based on an understanding of the molecular level processes continues to be an enduring goal for physical chemists. Molecular dynamics (MD) simulation method plays an increasingly important role in understanding the relationship between microscopic interactions and macroscopic physico-chemical properties. This is because MD simulation permits the researcher to selectively switch on and off key intermolecular interactions and evaluate their effect on the property of interest.

There have been a number of applications of MD simulation method to zeolite systems to investigate the local structure and dynamics of adsorbates in zeolite frameworks. For example, Demontis *et al.*, by using simple model potentials, reproduced the positions and vibrations of water molecules in the cages of natrolite,[1,2] the atomic coordinates and the crystal symmetry of dehydrated natrolite[3] and Linde zeolite 4A,[4] and their dynamical behavior in their MD simulation works. Further studies of the group included the diffusive motion of methane in silicate[5] and the structural changes of silicate at different temperatures by a MD method.[6] Cohen de Lara *et al.* also performed a MD study of methane adsorbed in zeolite A[7] based on their potential-energy calculation.[8] Other MD studies on time-dependent properties such as diffusion coefficients and intracrystalline site residence times were reported for methane in zeolite Y,[9] mordenite,[10] and ZSM-5,[10] for benzene in zeolite Y,[11] for water in ferrierite,[12-15] and for xenon,[16] methane, ethane, and propane in silicalite.[17] The dynamics of Na^+ ions inside a

*To whom correspondence should be addressed.

zeolite-A framework at several temperatures was described by a MD simulation by Shin *et al.*[18]

In our previous studies, we have performed molecular dynamics simulations of five different zeolite-A systems to investigate the structure and dynamics of adsorbates: rigid dehydrated zeolite-A,[19] two rigid Ca^{2+}-exchanged zeolite-A systems,[20] rigid hydrated zeolite-A,[21] rigid NH_4^+-exchanged zeolite-A,[22] and rigid H^+-exchanged and $CH_3NH_3^+$-exchanged zeolite-A[23] systems. The zeolite-A frameworks were assumed to be rigid and the framework atoms were fixed in the space at the positions determined by the X-ray diffraction experiments.[24-29]

The inclusion of the intraframework interaction of zeolite systems is essential to take account of energy exchange between the adsorbed molecules and the framework atoms and dynamical couplings of the sorbate with framework vibrations, as well as the flexibility of the host lattice. In a previous study,[30] an accurate valence force field for zeolite was presented by Nicholas *et al.* The force field contained terms for bond stretching, bond angle bending, torsional rotational, and Lennard-Jones and electrostatic non-bonded interactions. They found that the force field accurately reproduced the structure and dynamics of silica sodalite by the comparison of theoretical infrared (IR) spectra, radial distribution functions, and mean-square displacements with experimental data.

Recently Faux *et al.*[31] reported MD simulations of fully hydrated and dehydrated Na^+-zeolite 4A with a mobile zeolite framework at 298 K and a steepest descent energy minimization simulation on the dehydrated zeolite. They found that the optimized structure yielded bond lengths, bond angles, and positions of sodium ions in very good agreement with published X-ray data.[24,32] In fact, after our present work was begun, they published this report, but our work differs in the interaction potentials for the framework atoms.

Continuing our MD simulation studies of zeolite-A systems with rigid zeolite-A frameworks,[19-23] we present MD simulation of non-rigid zeolite-A framework only as the base case for a consistent study of the role of intraframework interaction on several zeolite-A systems. The primary purpose of this work is to provide the basic non-rigid zeolite-A framework, to test several intraframework interaction of zeolite A, and to investigate the local structure and dynamics of the non-rigid zeolite-A framework atoms. In Section II we present the molecular models and MD simulation method. We discuss our simulation results in Section III and present the concluding remarks in Section IV.

Molecular Models and Molecular Dynamics Simulations

The structure of zeolite-A framework is modeled by the pseudo cell, $(SiAlO_4)_{12}$, using the space group Pm3m (a= 12.2775 A). The Si and Al atoms are assumed to be identical (denoted as T) because the Ewald summation[33] is valid with this assumption. In this work, we consider the MD simulation of zeolite-A framework only and so there is no adsorbate. Since the zeolite-A framework is not assumed to be rigid, the framework atoms (T and O) are subject to move according to the equation of motion. For the initial positions of the framework atoms, those determined by the X-ray diffraction experiment of Pluth and Smith[24] for the dehydrated zeolite-A system are used.

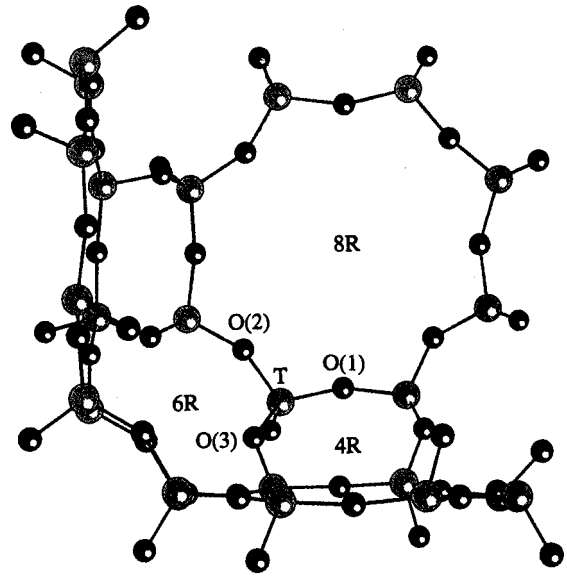

Figure 1. A snapshot of the pseudo cell of zeolite-A framework only. The structure is a little distorted because of non-rigidity.

The structure of the modeled zeolite-A framework is built up by the corner-sharing of TO_4 tetrahedra: a T atom is connected to four O atoms and an O atom is connected to two T atoms which gives a V-shape connection. The pseudo cell of the simulated zeolite-A framework is provided in Figure 1. The true unit cell of zeolite A is consist of 8 pseudo cells. The arrangement of oxygen atoms in zeolite A produces eight-membered (8R), six-membered (6R), and four-membered (4R) rings. α-cage is a cavity composed of six 8R, eight 6R, and twelve 4R on the faces, vertices, and edges of a cubic box, respectively, while β-cage is composed of eight 6R and eight 4R. There are eight α-cages and β-cages per unit cell. The oxygen atoms which are a member of 8R and 4R rings at the same time are labeled O (1), those of 8R and 6R labeled O(2), and those of 4R and 6R labeled O(3) and O(3').

The interaction potential for the framework atoms is given by the sum of bond stretching, bond angle bending, torsional rotational potential, and Lennard-Jones (LJ) and electrostatic non-bonded interactions. The usual LJ parameters and the electrostatic charges for the Coulomb potential are used in our previous studies[19-23] with the Ewald summation[33] and are given in Table 1. In the pseudo cell, $(TO_2)_{24}$, 24 T atoms, give a total of 96 T-O bonds. The T-O bond lengths of the TO_4 tetrahedra are different according to the O atoms: T-O(1)=0.16591, T-O(2)=0.16531, and T-O(3 or 3')=0.16688 nm. The T-O bond stretching potential is given by a simple harmonic potential[30]

$$V(r)=\frac{k_r}{2}(r_{T-O}-r_{eq})^2 \tag{1}$$

where k_r=250,000 kJ/mol·nm^2 and r_{eq}=0.16625 nm (the average of the above four T-O lengths).

Since each TO_4 tetrahedra gives 6 O-T-O angles, totally 144 O-T-O angles exist in the pseudo cell, $(TO_4)_{24}$. The O-

Table 1. Lennard-Jones parameters and electrostatic charges used in this study

Atom	σ (nm)	ε (kJ/mol)	Charge (e)
Al(=Si)	0.4009	0.5336	0.6081
O(1)	0.2890	0.6487	−0.4431
O(2)	0.2890	0.6487	−0.4473
O(3)	0.2890	0.6487	−0.4380

T-O angles are O(1)-T-O(2)=108.13, O(1)-T-O(3 or 3')= 111.70, O(2)-T-O(3 or 3')=107.12, and O(3)-T-O(3')=111.70 degrees. The O-T-O bond angle bending potential is also given by a simple harmonic potential

$$V(\theta)=\frac{k_\theta}{2}(\theta-\theta_{eq})^2 \quad (2)$$

where k_θ=0.17605 kJ/mol·deg^2 and θ_{eq}=109.43 degrees (the average of the above six O-T-O angles).

Each O atom gives a T-O-T angle and totally 48 T-O-T angles exist in the pseudo cell, $(TO_2)_{24}$. The T-O-T angles are T-O(1)-T=142.08, T-O(2)-T=164.18, and T-O(3 or 3')-T= 145.55 degrees. According to Nicholas *et al.*,[30] the T-O-T bond angle bending potential is given by an anharmonic potential

$$V(\theta)=\frac{k_{\theta 1}}{2}(\theta-\theta_{eq})^2+\frac{k_{\theta 2}}{2}(\theta-\theta_{eq})^3+\frac{k_{\theta 3}}{2}(\theta-\theta_{eq})^4 \quad (3)$$

where $k_{\theta 1}$=0.013829 kJ/mol·deg^2, $k_{\theta 2}$=0.00050542 kJ/mol·deg^3, $k_{\theta 3}$=0.000005148 kJ/mol·deg^4 and θ_{eq}=139.34 degrees (the average of the above four T-O-T angles).

In silicates the Si-O bond is known to lengthen as the Si-O-Si bond angle becomes smaller.[34] The exact relationship between the bond length and bond angle depends on the compound and also varies with the amount of Al in the lattice. In order to reproduce the correct dynamic behavior of the lattice, it is found that the Urey-Bradley term is needed based on the T-T non-bonded distance for each T-O-T angle[30]

$$V(r)=\frac{k_r}{2}(r_{T-T}-r_{eq})^2 \quad (4)$$

where k_r=22,845 kJ/mol·nm^2 and r_{eq}=0.31971 nm (the average of the following four T-T distances −0.31381, 0.32747, 0.31878, and 0.31878 nm).

In a dihedral angle which is associated to four consecutive atoms(O-T*-O*-T), a torsional rotational potentials on the T*-O* bond is possible since the three O atoms connected to T* except the O* atom are restricted by the O-T*-O angle bending potentials. In the pseudo cell, $(TO_2)_{24}$, there are 48 T-O-T angles. Since we can pick up one among three O atoms connected to each T atom to make a dihedral angle, it can make a total of 96 dihedral angles. The torsional rotational potential for the O-T-O-T dihedral angle is a periodic function with a 3-fold barrier:

$$V(\phi)=\frac{k_\phi}{2}[1+\cos(3\phi)] \quad (5)$$

where $k\phi$= − 2.9289 kJ/mol.

A canonical ensemble of fixed N (number of particles), V (volume of fixed zeolite-A framework), and T (temperature) is chosen for the simulation ensemble. Gauss's principle of least constraint[35] is used to maintain the system at a constant temperature. The ordinary periodic boundary condition in the x-, y-, and z-direction and minimum image convention are applied for the Lennard-Jones potential with a spherical cut-off of radius equal to the half of each simulation box length. Gear's fifth order predictor-corrector method[36] is used to solve the equations of translational motion of the framework atoms with a time step of 2.00×10^{-16} sec. The equilibrium properties are averaged over five blocks of 100,000 time steps, for a total of 500,000 time steps after 500,000 time steps to reach an equilibrium state. The configuration of each ion is stored every 5 time steps for further analyses. Several potential energies are averaged for 500,000 time steps (100 ps) and are listed in Table 2.

Table 2. Average potential energies (kJ/mol) for 500,000 time steps (100 ps)

Interaction potential	Potential energy
frame-frame LJ potential	−187.9±2.1
frame-frame Coulomb	2502.1±4.8
T-O bond stretching	133.3±8.2
T-T non-bond stretching	55.3±3.7
T-O-T bond angle bending	265.9±9.7
O-T-O bond angle bending	37.3±2.2
O-T-O-T torsional	−218.4±1.1

Results and Discussion

In Table 3, the results of the experimental[24] and calculated structural parameters of zeolite A are compared. The mean crystallographic positions and the mean-square displacement matrices B are obtained by referring the values of the individual atoms back to the asymmetric unit by symmetry operations.[37] The elements of the symmetric 3×3 matrix B are computed as $u_{ij}=<u_iu_j>=<r_ir_j>-<r_i><r_j>$. The agreement between the experimental and calculated coordinates is generally quite good with the mean deviation of 0.106 A. However, this value of the mean deviation is somewhat higher than those of Demontis *et al.*[4] when only the positions of the zeolite-A framework atoms are compared, probably due to the use of the average bond dis-

Table 3. Experimental[24] and calculated structural parameters of zeolite A

Atom	x/a	y/a	z/a	β_{11}	β_{22}	β_{33}	β_{12}	β_{13}	β_{23}
T									
exp.	0	0.1836	0.3722	38	35	26	0	0	5
cal.	0.0123	0.1792	0.3662	13.2	20.8	19.2	−3.4	−3.3	18.4
O(1)									
exp.	0	0.2275	0.5	65	76	28	0	0	0
cal.	0.0044	0.2049	0.4829	1.1	2.4	1.4	−0.5	0.0	0.1
O(2)									
exp.	0	0.2910	0.2910	90	48	48	0	0	22
cal.	0.0108	0.2932	0.2879	66.9	46.8	52.1	16.5	17.5	48.7
O(3)									
exp.	0.1119	0.1119	0.3437	52	52	56	11	3	3
cal.	0.1065	0.1065	0.3335	16.4	27.1	57.2	33.1	22.7	18.5

tances and bond angles in Eqs. (1)-(4). The anisotropy thermal parameters $\tilde{m}_{ij}$ can be used to visualize the extent of the thermal motions and their anisotropy by the ORATE computer code.[38] The values for O(1) are very small compared to those of the experiment.[24]

Figure 2 shows the radial distribution functions, g(r), of rigid and non-rigid zeolite-A framework atoms (a) between T and T, (b) between T and O, and (c) between O and O, respectively. The sharp peaks in the g(r) functions of rigid zeolite-A framework are due to the positional symmetry of the framework atoms. In contrast to these, those functions of non-rigid zeolite-A framework are broad due to the vibrational motions of the mobile framework atoms. When our g(r) functions of non-rigid zeolite-A framework atoms are compared with those of non-rigid silica sodalite framework atoms,[30] the results are much similar except that our g(r) functions have less structures. For example, in the T-T radial distribution of silica sodalite, there are seven distinct peaks out to the cut-off distance, but the overlap of distributions is appeared in the third peak. The first peaks at about 0.32, 0.17, and 0.27 nm in non-rigid zeolite-A framework are well defined, corresponding to the non-bonded or bonded T-T, T-O, and O-O distances, respectively.

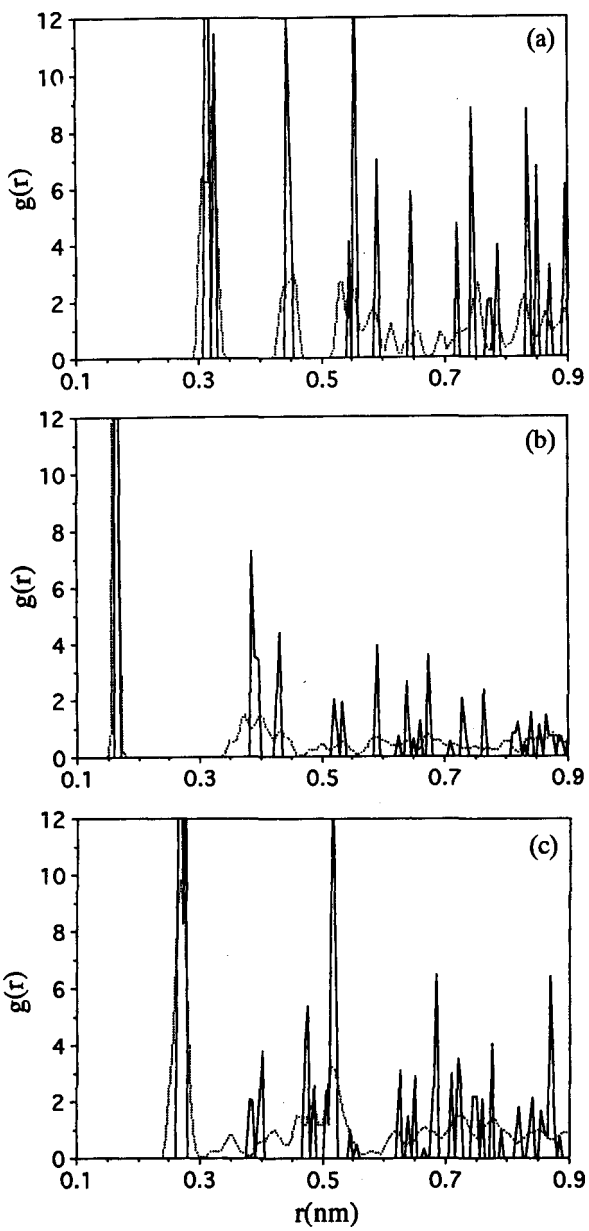

Figure 2. (a) T-T radial distribution function, (b) T-O radial distribution function, and (c) O-O radial distribution function in rigid (—) and non-rigid (···) zeolite-A frameworks.

Mean square displacements (MSD) of non-rigid zeolite-A framework atoms -T, O(1), O(2), and O(3)- are plotted in Figure 3. In a word, the MSD's are all periodic. This means that the four atoms go back and forth from their reference points at the same period but not at the same time. In other words, they do not always go far away and come near at the same time. Time-correlations in the displacements of these atoms will be discussed in the below. The amplitude of the MSD for T is somewhat less than those for O atoms probably due to the mass of T. However, the MSD for O(2) displays a much similar behavior to that for T. The periodic behavior of the MSD's for O(1) and O(3) is two-fold: a rapid vibrational motion with a short period of 0.08 ps and a slow change in the amplitude of the vibration with a long period of 0.53 ps.

In order to investigate the dynamical couplings between the zeolite-A framework atoms, we define a time-correlation function in the displacement of a certain atom respect to that of another atom from a reference point:

$$D_{ij}(t) = \langle \theta_i(0) \cdot \theta_j(t) \rangle \tag{6}$$

where $\theta(t)$ is the Heaviside step function, which is 1 if atom i goes far away from a reference point and -1 if it comes near to the point at time t. When $i=j$, we call it as a displacement auto-correlation (DAC) function, and when $i \neq j$, as a displacement neighbor-correlation (DNC) function. In the present study, we consider two kinds of reference points -the center of α-cage and the center of each window. For example, in the displacements of the three atoms at a 8-ring window in Figures 4 and 5, Figure 4 represents the displacements from the center of α-cage which consider the up-and-down motions from the 8-ring window plane and Figure 5 represents the displacements from the center of the 8-ring window which consider the back-and-forth motions on the plane (Figure 6).

Figure 4 (a) shows the DAC functions of T, O(1), and O

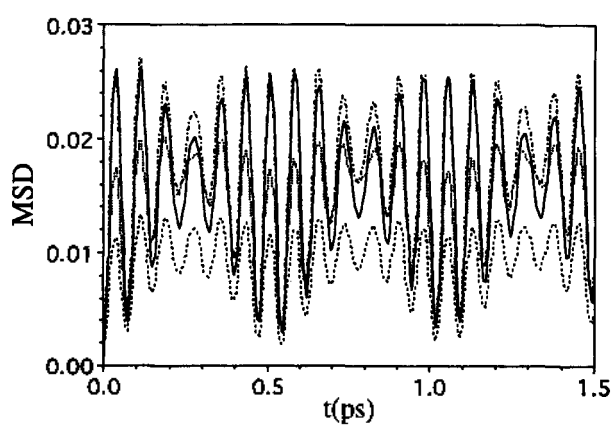

Figure 3. Mean square displacements of four atoms in non-rigid zeolite-A framework. ---: T, —: O(1), ···: O(2), and —·—·—: O(3).

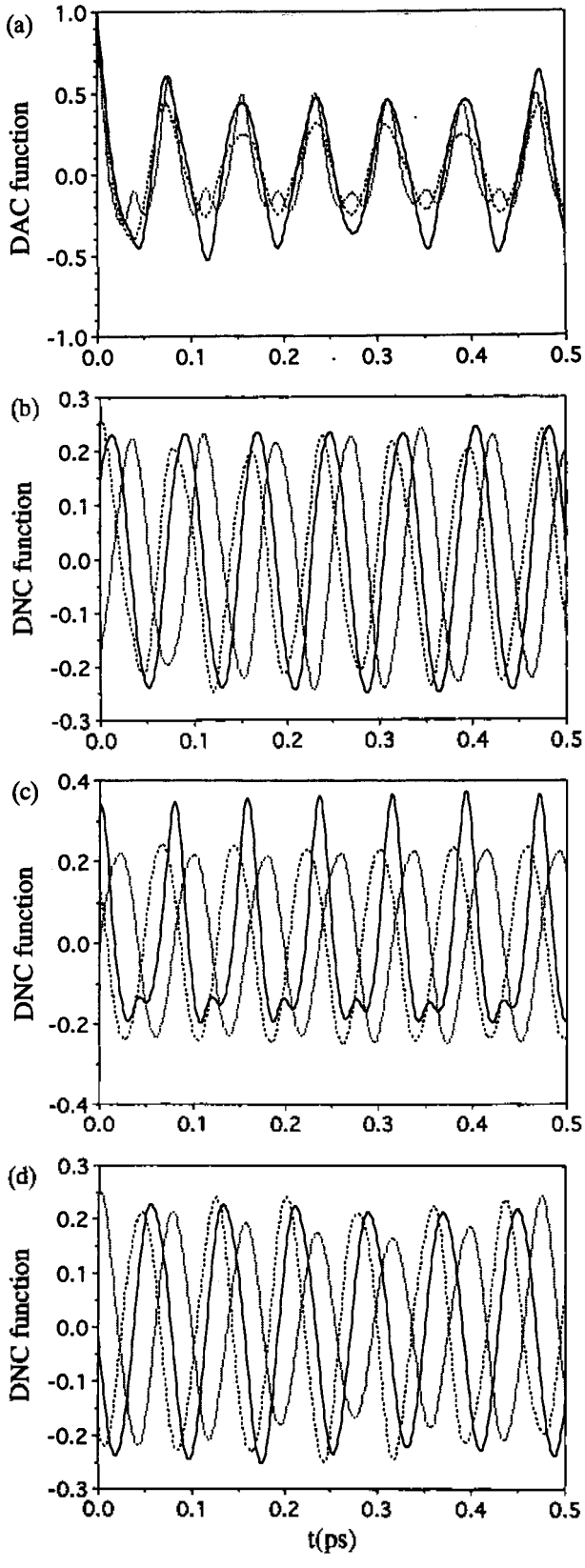

Figure 4. (a) Displacement auto-correlation functions of T (—), O(1) (---), and O(2) (···), and displacement neighbor-correlation functions of (b) T-T (—), T-O(1) (---), and T-O(2) (···), (c) O(1)-T (—), O(1)-O(1) (---), and O(1)-O(2) (···), and (d) O(2)-T (—), O(2)-O(1) (---), and O(2)-O(2) (···) from the center of α-cage at the 8-ring windows in non-rigid zeolite-A framework.

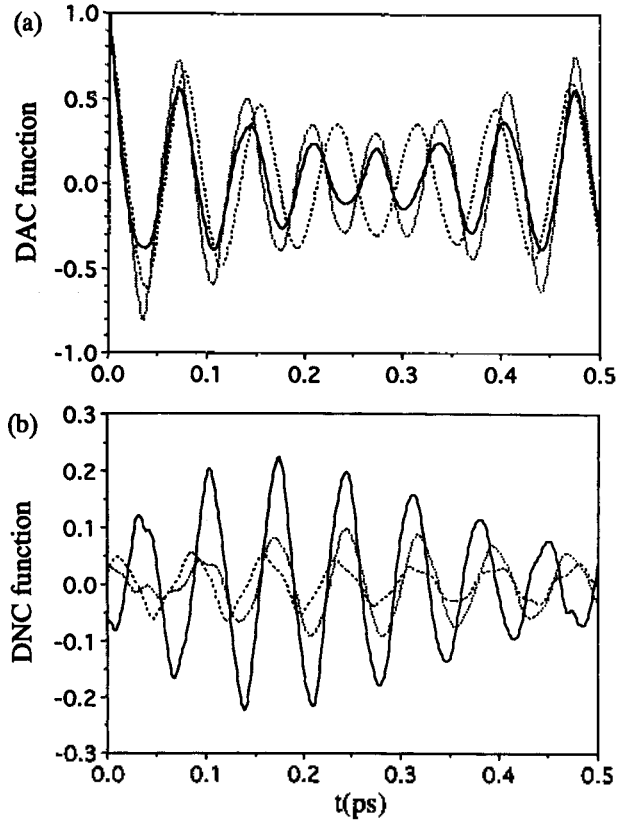

Figure 5. (a) Displacement auto-correlation functions of T (—), O(1) (---), and O(2) (···), and displacement neighbor-correlation functions of (b) O(1)-T (—), O(1)-O(1) (---), and O(1)-O(2) (···) from the center of 8-ring at the 8-ring windows in non-rigid zeolite-A framework.

(2) atoms at the 8-ring windows from the center of α-cage. All the three kinds of atoms are moving up-and-down from the 8-ring window plane with the period of 0.08 ps which is equal to that of the rapid vibrational motion in the MSD. However, this does not mean that all the three kinds of atoms go far away from the center of α-cage and come back near to the center at the same time. In order to see the time-direction table, we have to look at the DNC functions. From Figure 4 (b), at time t=0, respect to the motion of T atom, the other T atoms and O(1) atoms are moving to the same direction and O(2) atom in the opposite direction. The moving directions of these atoms are changed in the opposite direction very soon with the same period of changing direction. Figures 4 (c) and (d) show the DNC functions of T, O(1), and O(2) atoms respect to O(1) atom and of T, O (1), and O(2) atoms respect to O(2) atom, respectively.

In Figure 5 (a), the DAC functions of T, O(1), and O(2) atoms at the 8-ring windows from the center of 8-ring are plotted. O(2) atoms are moving back-and-forth on the 8-ring window plane with the period of 0.08 ps which is equal to that of up-and-down motion of the three atoms from the center of α-cage, but the back-and-forth motion of T and O(1) atoms is a little faster than that of O(2) atom. In Figure 5 (b), the DNC functions, respect to the motion of O (1) atom, of T, O(1), and O(2) atoms at the 8-ring windows from the center of 8-ring are plotted. At time t=0, T atoms are moving back-and-forth in the opposite direction to those

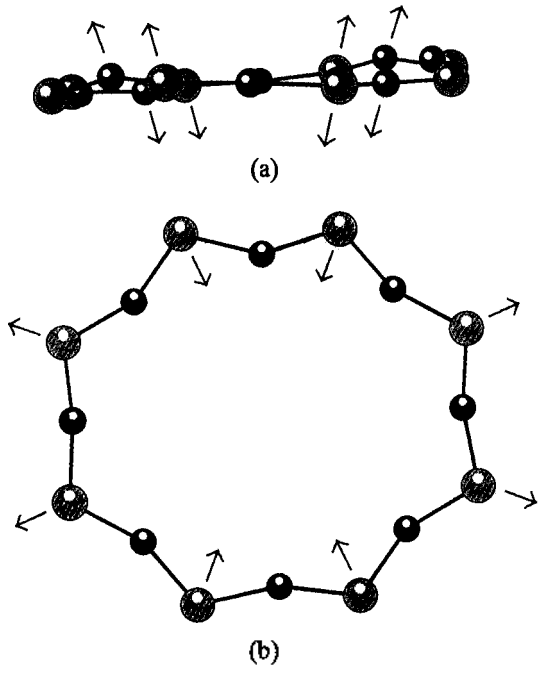

Figure 6. (a) Up-and-down motion of the 8-ring atoms from the center of α-cage and (b) back-and-forth motion of those atoms from the center of 8-ring window.

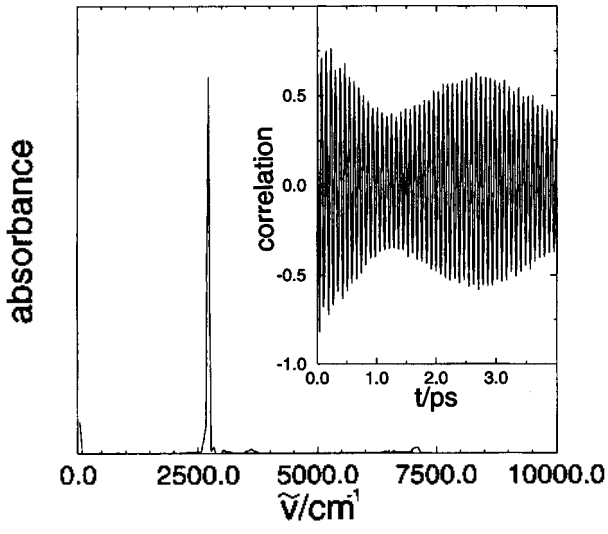

Figure 7. IR spectra of zeolite A, calculated from the total dipole moment autocorrelation function of zeolite-A framework (inset).

of O(1) and O(2) atoms respect to the motion of O(1) atoms, becoming in the same direction at the intermediate time, and then returning in the opposite direction at t=0.4 ps. This is mainly due to the different period of each atom in changing the direction of motion. It is worth noting that in Figure 4, the periods of up-and-down motion of all the atoms from the center of α-cage at the 8-ring windows are equal to one another. The DAC and DNC functions of the framework atoms from the center of α-cage and the centers of 6-ring and 4-ring windows at the 6-ring and 4-ring windows (not shown) display rather similar character to those of Figure 5 with different periods of motion. It will be interesting how the adsorbate such as Na^+ ion affects the vibrational motion of the non-rigid zeolite-A framework atoms.[39]

The IR spectrum is calculated by Fourier transformation of the total dipole moment autocorrelation function.[40] Figure 7 shows the total dipole moment autocorrelation function and the calculated IR spectra of zeolite-A framework from our MD simulation. The simple harmonic oscillation of the correlation function results in a large peak at 2700 cm^{-1} which reflects a monotonous dynamical feature of the framework.

Concluding Remarks

A molecular dynamics (MD) simulation of non-rigid zeolite-A framework only have been performed at 298.15 K. The reproduced positions of the zeolite-A framework atoms by our MD simulation are in quite good agreement with those of the experiment. The radial distribution functions and mean square displacements of the non-rigid zeolite-A framework atoms characterize the vibrational motion of the framework atoms. The up-and-down motion of the framework atoms from the center of α-cage and the back-and-forth motion on each ring window from the center of each window are well described by the displacement auto-correlation (DAC) and neighbor-correlation (DNC) functions. The introduction of the adsorbate such as Na^+ ion and its affection on the vibrational motion of the non-rigid zeolite-A framework atoms will be presented in a future publication.

Acknowledgment. This work was supported by a research grant (KOSEF 951-0302-026-2) to SHL from the Korea Science and Engineering Foundation. The authors thank to the Computer Center at Korea Institute of Science and Technology for the access to the Cray-C90 system.

References

1. Demontis, P.; Suffritti, G. B.; Alberti, A.; Quartieri, S.; Fois, E. S.; Gamba, A. *Gazz. Chim. Ital.* **1986**, *116*, 459.
2. Demontis, P.; Suffritti, G. B.; Quartieri, S.; Fois, E. S.; Gamba, A. *Dynamics of Molecular Crystals*; Lascombe, J. Ed.; Elsevier; Amsterdam; 1987; p 699.
3. Demontis, P.; Suffritti, G. B.; Quartieri, S.; Fois, E. S.; Gamba, A. *Zeolites* **1987**, *7*, 522.
4. Demontis, P.; Suffritti, G. B.; Quartieri, S.; Fois, E. S.; Gamba, A. *J. Phys. Chem.* **1988**, *92*, 867.
5. Demontis, P.; Fois, E. S.; Suffritti, G. B.; Quartieri, S. *J. Phys. Chem.* **1990**, *94*, 4329.
6. Demontis, P.; Suffritti, G. B.; Quartieri, S.; Gamba, A.; Fois, E. S. *J. Chem. Soc., Faraday Trans.* **1991**, *87*, 1657.
7. Cohen de Lara, E.; Kahn, R.; Goulary, A. M. *J. Chem. Phys.* **1989**, *90*, 7482.
8. Cohen de Lara, E.; Kahn, R. *J. Phys. Chem.* **1981**, *42*, 1029.
9. Yashonath, S.; Demontis, P.; Klein, M. L. *Chem. Phys. Lett.* **1988**, *153*, 551.
10. den Ouden, C. J. J.; Smit, B.; Wielers, A. F. H.; Jackson, R. A.; Nowak, A. K. *Mol. Sim.* **1989**, *4*, 121.
11. Yashonath, S.; Demontis, P.; Klein, M. L. *J. Phys. Chem.* **1989**, *93*, 5016.
12. Leherte, L.; Lie, G. C.; Swamy, K. N.; Clementi, E.; Derouane, E. G.; Andre, J. M. *Chem. Phys. Lett.* **1988**,

145, 237.
13. Leherte, L.; Andre, J. M.; Vercauteren, D. P.; Derouane, E. G. *J. Molec. Catal.* **1989**, *54*, 426.
14. Leherte, L.; Andre, J. M.; Derouane, E. G.; Vercauteren, D. P. *Comput. Chem.* **1991**, *15*, 273.
15. Leherte, L.; Andre, J. M.; Derouane, E. G.; Vercauteren, D. P. *J. Chem. Soc., Faraday Trans.* **1991**, *87*, 1959.
16. Pickett, S. D.; Nowak, A. K.; Thomas, J. M.; Peterson, B. K.; Swift, J. F. P.; Cheetham, A. K.; den Ouden C. J. J.; Smit, B.; Post, M. F. M. *J. Phys. Chem.* **1990**, *94*, 1233.
17. Nowak, A. K.; den Ouden C. J. J.; Pickett, S. D.; Smith, B.; Cheetham, A. K.; Post, M. F. M.; Thomas, J. M. *J. Phys. Chem.* **1991**, *95*, 848.
18. Shin, J. M.; No, K. T.; Jhon, M. S. *J. Phys. Chem.* **1988**, *92*, 4533.
19. Moon, G. K.; Choi, S. G.; Kim, H. S.; Lee, S. H. *Bull. Kor. Chem. Soc.* **1992**, *13*, 317.
20. Moon, G. K.; Choi, S. G.; Kim, H. S.; Lee, S. H. *Bull. Kor. Chem. Soc.* **1993**, *14*, 356.
21. Lee, S. H.; Moon, G. K.; Choi, S. G.; Kim, H. S. *J. Phys. Chem.* **1994**, *98*, 1561.
22. Choi, S. G.; Lee, S. H. *Mol. Sim.* **1996**, *17*, 113. In Figs. 2, 3, 4, and 5, NH4(2) and NH4(3) should be replaced by each other.
23. Lee, S. H.; Choi S. G. *J. Phys. Chem.* B **1997**, *101*, 8402.
24. Pluth, J. J.; Smith, J. V. *J. Am. Chem. Soc.* **1980**, *102*, 4704.
25. Pluth, J. J.; Smith, J. V. *J. Am. Chem. Soc.* **1983**, *105*, 1192.
26. Jang, S. B.; Han, Y. W.; Kim, D. S.; Kim, Y. *Kor. J. Crystal.* **1990**, *1*, 76.
27. Seff, K.; Shoemaker, D. P. *Acta Crystallogr.* **1967**, *22*, 162
28. Gramlich, V.; Meier, W. M. *Z. Kristallogr.* **1971**, *133*, 134.
29. McCusker, L. B.; Seff, K. *J. Am. Chem. Soc.* **1981**, *103*, 3441.
30. Nicholas, J. B.; Hopfinger, A. J.; Trouw, F. R.; Iton, L. X. *J. Am. Chem. Soc.* **1991**, *113*, 4792
31. Faux, D. A.; Smith, W.; Forester, T. R. *J. Phys. Chem.* B **1997**, *101*, 1762.
32. Yanagida, R. Y.; Amaro, A. A.; Seff, K. *J. Phys. Chem.* **1973**, *77*, 805.
33. (a) de Leeuw, S. W.; Perram, J. W.; Smith, E. R. *Proc. R. Soc. London* **1980**, *A373*, 27. (b) Anastasiou, N.; Fincham, D. *Comput. Phys. Commun.* **1982**, *25*, 159.
34. Genechten, K. A. V.; Mortier, W. J. *Zeolites* **1988**, *8*, 273.
35. Gauss, K. F. *J. Reine. Angew. Math.* **1829**, *IV*, 232.
36. Gear, C. W. *Numerical initial value problems in ordinary differential equation*; Englewood Cliffs NJ; Prentice-Hall, 1971.
37. Willis, B. T. M.; Pryor, A. W. *Thermal vibrations in Crystallography*; Cambridge University Press; Cambridge, 1975.
38. Johnson, C. K. ORTEP: A FORTRAN *Thermal Ellipsoid Plot Program*; ORNL-3794, Oak Ridge National Laboratory, Oak Ridge, TN, 9165.
39. Lee, S. H.; Choi, S. G. in preparation.
40. Behrens, P. H.; Wilson, K. R. *J. Chem. Phys.* **1981**, *74*, 4872.

Thermal Decomposition of PVB (polyvinyl butyral) Binder in the MCFC (molten carbonate fuel cell)

Jung Ju Seo*, Ji Young Kim†, and Keon Kim†

Korea Basic Science Institute Seoul Branch, 126-16 Anam-dong, Sungbuk-Ku, Seoul 136-701, Korea
†Department of Chemistry, Korea University, 1 Anam-dong, Sungbuk-Ku, Seoul 136-701, Korea
Received November 1, 1997

The thermal decomposition of matrix-green sheet and electrolyte-green sheet in CO_2, sintering effect of Ni-green sheet for the decomposition of matrix-green sheet, and binder burnout during MCFC unit cell operation were studied. Binders decomposed incompletely in CO_2 and thermal decomposition of electrolyte-green sheet was affected more than that of matrix-green sheet by CO_2. It was important to decompose the binder completely before it changed to nonoxidative condition. Binders were more effectively eliminated in the sintered Ni-matrix green sheet than Ni-matrix green sheet. The decomposition state of binder during unit cell operation was showed by analyzing the produced gases. Two characteristic peaks, butanal and butene were detected at all experimental condition and binder burnout state was checked by analyzing the change of two index peaks during decomposition process. Most of binders in the unit cell were decomposed sufficiently under slow heating rate and initial oxidative condition.

Introduction

A fuel cell is a device that directly converts the chemical energy of reactants into electric energy by electrochemical reactions. Molten carbonate fuel cells (MCFCs) are presently under development for electric utility power generation.